IOP Conf. Series: Materials Science and Engineering **275** (2017) 012041 doi:10.1088/1757-899X/275/1/012041

High Strain Rate Response of 7055 Aluminum Alloy Subject to Square-spot Laser Shock Peening

Rujian Sun, Ying Zhu, Liuhe Li, Wei Guo and Peng Peng

School of Mechanical Engineering and Automation, Beihang University, Beijing, 100191, China
E-mail address: sunrujian@buaa.edu.cn

Abstract: The influences of laser pulse energy and impact time on high strain rate response of 7055 aluminum alloy subject to square-spot laser shock peening (SLSP) were investigate. Microstructural evolution was characterized by OM, SEM and TEM. Microhardness distribution and in-depth residual stress in 15 J with one and two impacts and 25 J with one and two impacts were analyzed. Results show that the original rolling structures were significantly refined due to laser shock induced recrystallization. High density of microdefects was generated, such as dislocation tangles, dislocation wall and stacking faults. Subgrains and nanograins were induced in the surface layer, resulting in grain refinement in the near surface layer after SLSP. Compressive residual stresses with maximum value of more than -200 MPa and affected depths of more than 1 mm can be generated after SLSP. Impact time has more effectiveness than laser pulse energy in increasing the magnitude of residual stress and achieving thicker hardening layer.

1. Introduction

Laser shock peening (LSP), also called laser shock processing, is an innovative surface treatment technique, which has been widely employed to enhance fatigue, corrosion and wear resistance of metallic components served in aerospace engineering [1-3]. Comparing to shot peening (SP), the compressive residual stress layer introduced by LSP is 2-5 times thicker than that generated by SP [4]. LSP applies a high power density (in GW cm^{-2} range), ultra-short duration (tens of nanoseconds) pulse laser to the surface of metallic materials, forming plasma that reaches a temperature higher than 10000°C and generating a high pressure shock wave (in GPa range). The interaction between shock wave and target material will generate high density of microdefects, induce grain refinement and modify near surface residual stress field [5].

According to the shape of laser spot, LSP can be divided into circular-spot laser shock peening (CLSP) and square-spot laser shock peening (SLSP) [6]. In a typical SLSP process, laser energy distributes homogeneously in the square spot after adjusting spot shape using beam homogenizer. SLSP can treat a large area effectively with the overlapping ratio less than 10% [7]. Cao et al. reported that surface morphology produced by square laser spots was smoother than that produced by circular spots [8]. In addition, square laser spot can effectively avoid the phenomenon of residual stress hole. Hu et al. studied the non-homogeneity of residual stress field and found that the residual stress drop in a square laser spot was less severe than that in a circular laser spot [9]. However, little open literature pays attention to the microstructural evolution, mechanical property and experimental residual stress field of materials under SLSP.

In this study, SLSP was carried out to investigate high strain rate response of 7055 aluminum alloy, focusing on microstructural evolution, microhardness distribution and residual stress field. Different laser pulse energy and impact times were examined to offer a better understanding of material response under SLSP. It is believed that this study can provide a new insight for widening LSP technique in both scientific and industrial application.

2. Experiments

2.1. Experimental Procedure

In this study, 7055 aluminum alloy was selected in this work with a full chemical composition listed in Table.1. It is initially developed by Alcoa in 1980s, and is mainly applied as envelope of horizontal tail and other parts. The samples were cut into a rectangular plate with dimensions of 50 mm×30 mm×5 mm (length × width × thickness). Before SLSP, all samples were first ground with SiC paper from 150 # to 2000 # and then rinsed with deionized water by ultrasonic vibration. Shortly after the preparation, SLSP was performed in water confinement using a Q-switched Nd:YAG laser operating in a wavelength of 1064 nm, pulse width of 15 ns and a repetitive frequency of 1 Hz. The focused laser presents a 4 mm square spot after beam homogenization. All specimens were protected from the thermal effects of SLSP by a 100 μm aluminum foil (made by 3M). Two kinds of pulse energies of 15 and 25 J and impact time of one and two were selected for SLSP experiments. The laser path was a zigzag covering an area of 40 mm × 20 mm. The overlapping rate (ov %) represents percentage of the overlapped length in center distance of two adjacent laser spot. Thereby, an overlapping rate of 15% was adopted. The laser path and overlapping illustration are shown in Figure 1.

Table 1. Chemical compositions of 7055 aluminum alloy (wt %)

Cu	Mg	Zn	Zr	Fe	Mn	Si	Al
2.0 - 2.6	1.8 - 2.3	7.6 - 8.4	0.08 - 0.25	≤0.15	≤0.05	≤ 0.10	Bal.

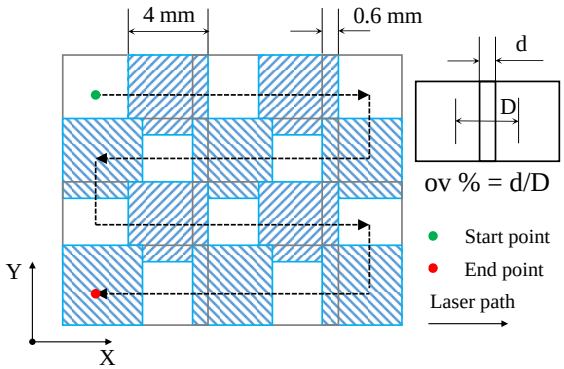

Figure 1. Laser path illustrating an overlapping rate of 15%.

2.2. Material Characterization

Optical Microscope (ASA1, Zeiss) and Scanning Electron Microscopy (SEM) were used to observe microstructure features of samples before and after SLSP. Prior to the observation, cross section of each sample was ground to 2500 # and then mechanically polished before etched by Keller's reagent (95 mL H_2O, 2.5 mL HNO_3, 1.5 mL HCl and 1 mL HF). In addition, Polarized Light Microscopy (PLM) was employed to reveal the grain structure after anodic oxidation with Barker's reagent (97.5 mL H_2O, 2.5 mL HBF_4). Transmission electron microscope (TEM, JEM-2100, JEOL), operated at 200 kV, was employed to investigate microstructural evolution of samples after SLSP. The sample was cut into a 0.5 mm thickness sheet and afterwards mechanically ground and polished down to about 100

μm thickness. The 100 μm sheet was punched out to 3 mm diameter discs, followed by ion-milling by Ar + bombardment with proper incident angles.

Micro-vickers hardness tester (FUTURE-TECH, FM-800) was adopted to study the variety of microhardness from SLSP treated surface down to the base metal with a step distance of 100 μm, test weight of 200 g, and dwell time of 10 s. To eliminate the deviation, each measure was repeated for three times and the average values were presented in this study. Prism residual stress measurement system based on incremental hole drilling method was applied to measure residual in the depth direction of specimen before and after SLSP. It is a destructive residual stress measurement. Residual stresses were measured from the surface to a depth of 1 mm.

3. Results and Discussion

3.1. Microstructure

Figure 2 presents PLM and SEM images of the sample before SLSP, which show clear rolling structures. Longish grains in both PLM and SEM images are confirmed.

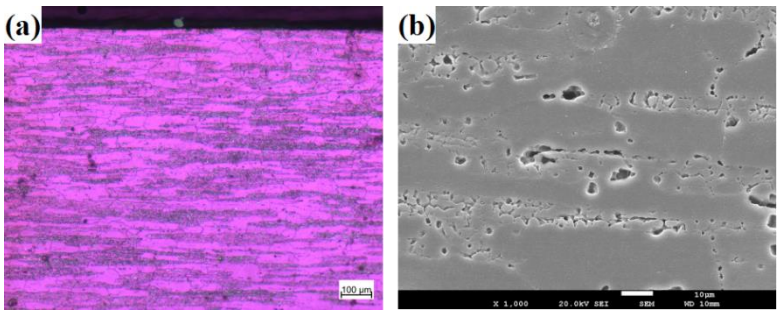

Figure 2. Microstructure before SLSP. (a) OM image and (b) SEM image.

Figure 3 and Figure 4 illustrate PLM and SEM images of the samples after SLSP, respectively. Figure 3(a) and (b) expound microstructural evolution under 15 J with one and two impacts. The continuous longish grains broke into intermittent smaller grains and further into randomly oriented fragmentary grains after one and two impacts. Similar results were reported by Trdan et al. who found randomly distributed smaller grains on the LSPed surface layer and oriented longish grains in the center of sample [10] Figure 3(c) and (d) show microstructural evolution under 25 J with one and two impacts. The density and the length of such longish grains decreased when increasing laser energy from 15 to 25 J. In addition, recrystallization of longish grains can also be observed. Randomly oriented net-like grains can be discovered after 25 J SLSP with two impacts. Lu et al. point out that a severe plastic deformation layer was generated near the top surface during LSP, and the grains in the severe plastic deformation layer were significantly refined [11].

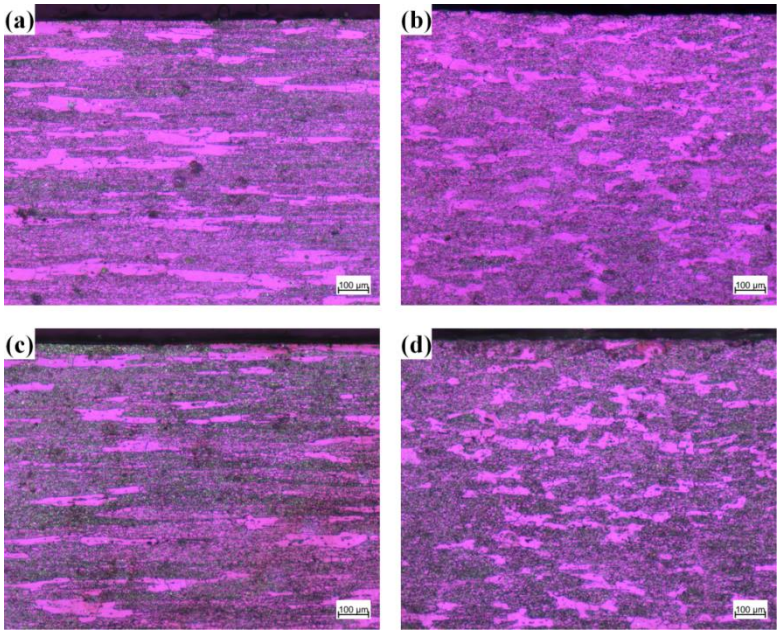

Figure 3. Microstructural evolution after SLSP under PLM. (a) 15 J with one impact; (b) 15 J with two impacts; (c) 25 J with one impact and (d) 25 J with two impacts.

Figure 4 shows SEM images, which confirm the presence of recrystallized grains in samples after SLSP. Longish grains still can be observed in Figure 4(a). However, the longish grain broke into intermittent smaller grains with the grain sizes varying from 2 μm to 20 μm, as shown in Figure 4(b), when the sample was subject to 15 J SLSP. When the samples are treated by 25 J with one and two impacts, small equiaxed grains can be obtained. The average grain in Figure 4(d) is about 5-8 μm.

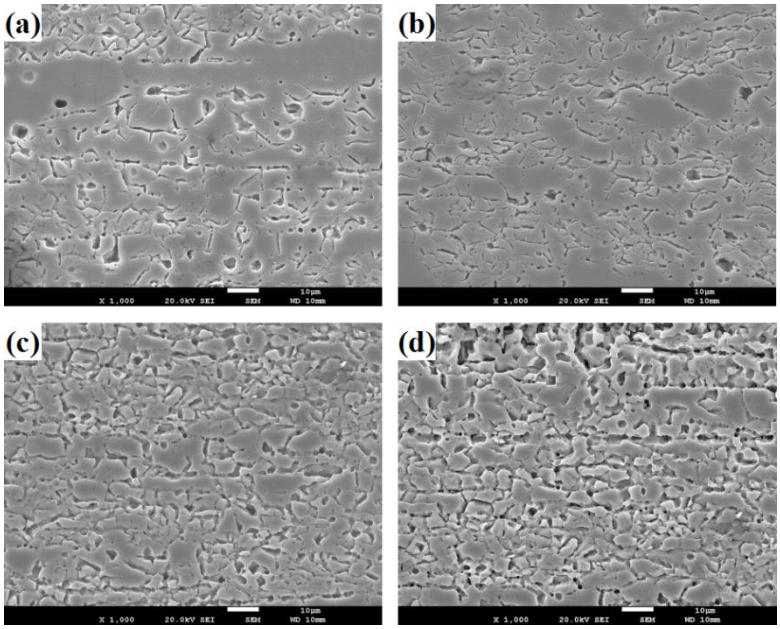

Figure 4. Microstructural evolution after SLSP under SEM. (a) 15 J with one impact; (b) 15 J with two impacts; (c) 25 J with one impact and (d) 25 J with two impacts.

Hence, it can be concluded from both PLM and SEM images that SLSP is an effective method to generate refined grains in the treated region, which can be favorable to the improvement on the fatigue life of 7055 aluminum alloy.

Figure 5 shows typical TEM images of samples treated by SLSP with laser energy of 15 J. From Figure 5(a), it can be clearly observed that a large number of microdefects randomly distributed in the grain, such as dislocation tangles and dislocation walls. However, no obvious observation of dislocation lines, which can be attribute that the surface layer was severely deformed during the SLSP process that dislocation lines slipped and multiplicated into dislocation tangles and wall [12]. Figure 5(b) present the image taken from the zone [A] in Figure 5(a). Stacking faults can be discovered in the edge of dislocation tangle and subgrain boundary between the dislocation tangle and original grain can also be detected. Figure 5(c) is the high-resolution transmission electron microscopy (HRTEM) image taken from ellipse [B] in Figure 5(b). Typical stack faulting structure spacing 0.606 nm can be observed in region [I] and periodic dislocation of atom arrangement in region [II] spaced 0.202 nm. Figure 5(d) presents details in ellipse [C] in Figure 5(b), in which a number of nanograins can be observed with its corresponding selected area electron diffraction (SEAD) being concentric circles. Its HRTEM is shown in Figure 5(e), in which the sizes of nanograins are about 20 to 30 nm. In addition, subgrains and subgrain boundary can be found in Figure 5(f), which are the very first step for the formation of refined grains.

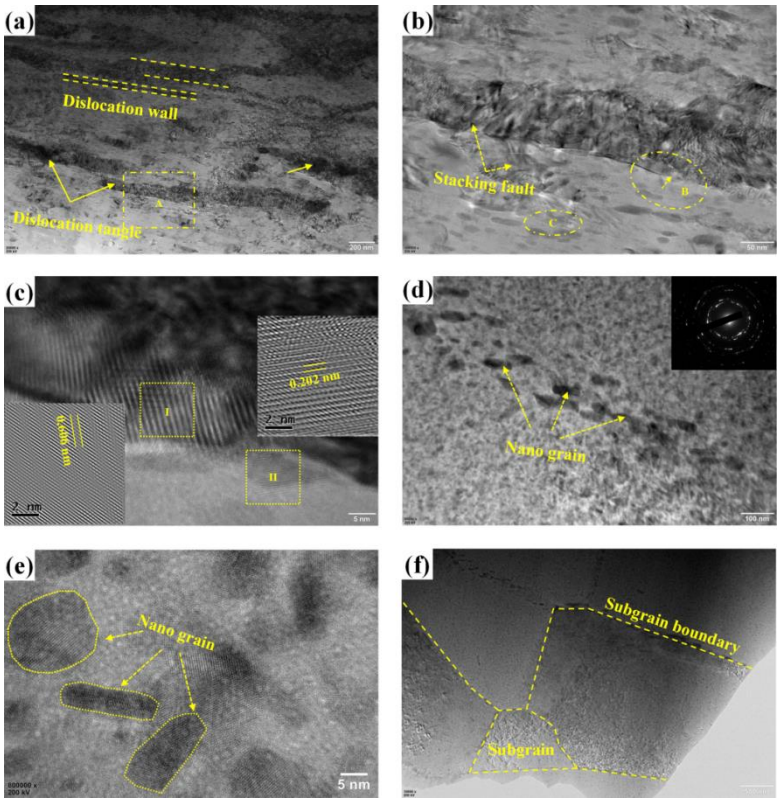

Figure 5. Typical TEM images after SLSP. (a) dislocation structures; (b) detail of zone [A] illustrating stack faults; (c) HRTEM taken from ellipse [B] in Figure 5(b); (d) detail of ellipse [C] in Figure 5(b) illustrating namograins; (e) HRTEM of nanograins and (f) surgrains and subgrain boundary.

3.2. Microhardness

Figure 6 presents a comparison of in-depth microhardness of samples before and after SLSP. It can be clearly found that SLSP can introduce a hardening layer within the top surface. It is also worth noting that the microhardness increment in SLSP is lower than that in conventional CLSP. This is due to low

magnitude of peak pressure resulted from different laser energy distribution in the spot. The laser energy distributes as Gaussian function in a circular spot, while it distributes homogeneously in a square spot. The net result is that the peak pressure in the center of a square spot is lower than that in a circular spot. As for surface microhardness, increasing laser pulse energy to 15 J and 20 J, surface microhardness increased by approximately 10 HV and 20 HV respectively comparing with original surface microhardness, while increasing impact time from one to two resulted in slight change of surface microhardness both in 15 J and 25 J SLSP. According to Hall-patch theory [13, 14], HV is proportional to $\rho^{1/2}$ (ρ, dislocation density). Therefore, the enhancement in microhardness is due to the generation of high-density dislocation.

As for the depth of hardening affected layer, increasing laser pulse energy to 15 J and 20 J, an affected depth of 780 μm and 1100 μm were obtained respectively. This is because SLSP-induced shock wave transmitted deeper in 25 J and interacted more intensively with the target material. When increasing impact time of peening in both 15 J and 25 J, the affected depths in both condition exceeded 1.3 mm. The affected depth generated by a square spot is deeper than that of a circular spot because the shock in a square spot expands like a planar front, which attenuates at a rate of 1/r, while in a circular spot the shock wave behaves like a sphere, which results in attenuation at a rate of $1/r^2$ [5, 10].

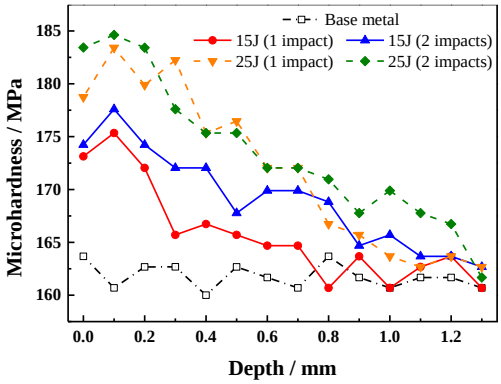

Figure 6. In-depth microhardness distribution after 15 J and 25 J SLSP with one and two impacts.

3.3. Residual Stress

Figure 7 exhibits the comparison of in-depth residual stresses after 15 J and 25 J SLSP with one and two impacts. It is clearly shown that compressive residual stresses with maximum value of several hundred MPa and affected depths of several hundred microns to more than 1 mm have been introduced in the surface and subsurface. The peak compressive residual stress increased from -120 MPa to -166 MPa, when increasing laser energy from 15 J to 25 J. Moreover, when increasing impact time from one to two in 15 J and 25 J, the compressive residual stress increased by 61.6% and 42.0% (from -120 MPa to -194 MPa and from -166 MPa to -234 MPa), respectively. The lower increment in 25 J can be attributed to the degree of residual stress saturation, which means the residual stress generated in 25 J is more saturated than that in 15 J with one impact. The more the generated stress is, the lower increment of the residual stress will be. As for the residual stress affected depth, it increased from ~700 μm to ~1 mm, when increasing laser pulse energy from 15 J to 25 J. The similar increments can also be achieved when increasing impact time from one to two in both 15 J and 25 J SLSP. Noting that the peak compressive residual stress in 15 J with two impacts is higher than that in 25 J with one impact, which proves that increasing impact time is a more effective method in acquiring high value residual stress. It is also worth noting that the peak compressive residual stresses are not located in the surface, but a depth between 100 μm to 200 μm. This is due to the release wave generated by boundary effect focalized to its center, causing reverse plastic strain and the stress drop [9].

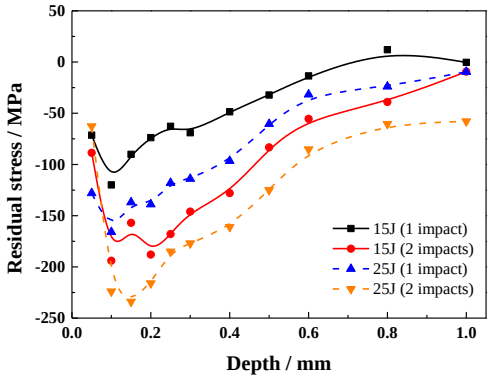

Figure 7. In-depth residual stress distribution after 15 J and 25 J SLSP with one and two impacts

4. Conclusions

Square-spot laser shock peening on 7055 aluminum alloy with laser energies of 15 J one and two impacts and 25 J one and two impacts has been investigated. The main findings are listed below.

- Microstructural PLM and SEM observations revealed that microstructures were significantly refined due to laser shock induced recrystallization. The longish rolling grains broke into intermittent smaller grains and further into randomly oriented fragmentary grains.
- Microdefects such as dislocation tangles, dislocation wall and stacking fault were generated in the surface layer after SLSP. Subgrains and nanograins were also obtained in the surface layer. These microdefects played a significant role in surface layer grain refinement.
- A higher value of surface microhardness can be achieved by increasing laser pulse energy, while increasing impact time only cause slight change in surface microhardness. However, thicker hardening layers can be obtained by increasing laser pulse energy or impact time. The hardening layer exceeded 1.3 mm in 25 J SLSP with two impacts.
- A higher value of peak residual stresses and thicker compressive residual stress layers can be achieved by increasing laser pulse energy and impact time. However, increasing impact time can be a more effective method in acquiring high peak residual stress.

Acknowledgement

The authors would like to acknowledge the support of this research work from the National International Collaborative Science and Technology Research Project China (Grant No. 2013DFR50590), and National Natural Science Foundation of China (Grant No. 11372019).

References

[1] Montross C S, Wei T, Ye L, Clark G and Mai Y W 2002 Laser shock processing and its effects on microstructure and properties of metal alloys: a review *International Journal of Fatigue* **24** 1021-36

[2] Nalla R K, Altenberger I, Noster U, Liu G Y, Scholtes B and Ritchie R O 2003 On the influence of mechanical surface treatments—deep rolling and laser shock peening—on the fatigue behavior of Ti–6Al–4V at ambient and elevated temperatures *Materials Science & Engineering A* **355** 216-30

[3] Yang J M, Her Y C, Han N and Clauer A 2001 Laser shock peening on fatigue behavior of 2024-T3 Al alloy with fastener holes and stopholes *Materials Science & Engineering A* **298** 296-9

[4] Ding K and Ye L 2006 *Laser shock peening: performance and process simulation*: Woodhead Publishing)

[5] Sun R, Li L, Zhu Y, Zhang L, Guo W, Peng P, Li B, Guo C, Liu L and Che Z 2017 Dynamic response and residual stress fields of Ti6Al4V alloy under shock wave induced by laser shock peening *Modelling & Simulation in Materials Science & Engineering* **25** 065016

[6] Ding K 2003 Three-dimensional Dynamic Finite Element Analysis of Multiple Laser Shock Peening Processes *Surface Engineering* **19** 351-8
[7] Kim T, Hwang S, Hong K H and Yu T J 2016 Analysis of the Square Beam Energy Efficiency of a Homogenizer Near the Target for Laser Shock Peening *Journal of the Optical Society of Korea* **20** 407-12
[8] Cao Z W, Gong S L and Gao Y 2013 Characterization of TC17 Titanium Alloy Treated by Square-Spot Laser Shock Peening *Advanced Materials Research* **654** 2378-83
[9] Hu Y, Gong C, Yao Z and Hu J 2009 Investigation on the non-homogeneity of residual stress field induced by laser shock peening *Surface & Coatings Technology* **203** 3503-8
[10] Trdan U, Skarba M and Grum J 2014 Laser shock peening effect on the dislocation transitions and grain refinement of Al–Mg–Si alloy *Materials Characterization* **97** 57-68
[11] Lu J Z, Luo K Y, Zhang Y K, Cui C Y, Sun G F, Zhou J Z, Zhang L, You J, Chen K M and Zhong J W 2010 Grain refinement of LY2 aluminum alloy induced by ultra-high plastic strain during multiple laser shock processing impacts *Acta Materialia* **58** 3984-94
[12] Lainé S J, Knowles K M, Doorbar P J, Cutts R D and Rugg D 2017 Microstructural characterisation of metallic shot peened and laser shock peened Ti–6Al–4V *Acta Materialia* **123** 350-61
[13] Chu J P, Rigsbee J M, Banaś G and Elsayed-Ali H E 1999 Laser-shock processing effects on surface microstructure and mechanical properties of low carbon steel *Materials Science & Engineering A* **260** 260-8
[14] Lu J Z, Wu L J, Sun G F, Luo K Y, Zhang Y K, Cai J, Cui C Y and Luo X M 2017 Microstructural response and grain refinement mechanism of commercially pure titanium subjected to multiple laser shock peening impacts *Acta Materialia* **127** 252-66